Title

Age-related changes of lens stiffness in wild-type and Cx46 knockout mice

Authors

Stopka, Wiktor
Libby, Tom
Lin, Stephanie
et al.

Publication Date

2021-11-01

DOI

10.1016/j.exer.2021.108777

Peer reviewed

HHS Public Access

Author manuscript

Exp Eye Res. Author manuscript; available in PMC 2023 March 29.

Published in final edited form as:

Exp Eye Res. 2021 November ; 212: 108777. doi:10.1016/j.exer.2021.108777.

Age-related changes of lens stiffness in wild-type and Cx46 knockout mice

Wiktor Stopka[a], **Tom Libby**[b], **Stephanie Lin**[c], **Eddie Wang**[c], **Chun-hong Xia**[c], **Xiaohua Gong**[a,c,*]

[a]UC Berkeley – UCSF Graduate Program in Bioengineering, University of California, Berkeley, CA, USA

[b]Center for Biological Inspiration in Education and Research (CiBER), University of California, Berkeley, CA, USA

[c]School of Optometry and Vision Science Program, University of California, Berkeley, CA, USA

Abstract

We have investigated how connexin 46 (Cx46) regulates lens stiffness by studying different Cx46 knockout (Cx46KO) mice. A modified muscle lever system was used to determine the lens stiffness of wild-type (WT) and Cx46KO mice at the C57BL/6J (B6) and the 129SvJae (129) strain backgrounds according to total lens displacement at the point of maximum force when fresh lenses were compressed with a maximum of 2 mN of force. In comparison to B6-WT controls, young and old B6-Cx46KO lenses showed 23% and 28% reductions in lens displacement, respectively. Comparing to 129-WT controls, old 129-Cx46KO lenses showed 50% reduction in the lens displacement while young 129-Cx46KO lenses displayed similar displacement. Old B6-Cx46KO and old 129-Cx46KO lenses showed almost identical lens displacement, 128 μm versus 127 μm. Morphological data revealed unique changes of peripheral fiber cell shapes in young B6-WT lenses but not in young B6-Cx46KO, 129-WT and 129-Cx46KO lenses. This work reveals Cx46 deletion increases the lens stiffness in both young and old mice at B6 strain background but only in old mice at 129 strain background which contains intermediate filament CP49 gene deletion. Cx46 impairment increases old mouse lens stiffness and may contribute to the development of presbyopia.

Keywords

Lens; Cataract; Aging; Connexin; Gap junction; Intermediate filament

*Corresponding author. University of California, 93 Minor Hall, Berkeley, CA, 94720, USA. xgong@berkeley.edu (X. Gong).

Author contribution

WS conducted the experiments and analyzed the results. TL generously provided the muscle lever device, offered advice on the design of the experiments, helped with Matlab coding, and advised how to analyze the data. SL helped to cut the vibratome sections. EW and CX provided several of the mice used in the study. WS, XG and CX wrote/edited the paper.

Declaration of Competing Interest

The authors declare no competing financial interests.

1. Introduction

The ability of the lens to change its shape to focus is called accommodation, which is related to lens stiffness. The stiffness of the eye lens has been shown to increase with age (Glasser and Campbell, 1999; Heys et al., 2004; Weeber et al., 2007). The increase in lens stiffness has also been suggested to be one of the causes for presbyopia, named for the age-related decrease in the ability of the lens to focus for near vision. Presbyopia will affect everyone with age, so a better understanding about the mechanistic regulation of lens stiffness in aging may lead to potential strategies to delay the onset of this vision disorder to occur later in life.

Several changes may lead to increased stiffness of the aging lens (Baradia et al., 2010; Wang and Pierscionek, 2019). For instance, the lens continues to grow in size by adding additional layers of fiber cells to the outside bulk of the lens (Cheng et al., 2019). Aging is associated with an accumulation of post-translational modifications of long-lived lens crystallin proteins as well as increased oxidative damage and cross-linking of lens cytoskeletal proteins that may impact on the mechanical properties of lens inner mature fibers (Nandi et al., 2020). However, the underlying molecular and cellular mechanisms for regulating lens stiffness, accommodation and presbyopia remain poorly understood.

Although mice lack fully developed ciliary muscles and mouse lenses do not accommodate like the primate lens, mice have similar cellular architecture for lens stiffness and transparency that can be measured in vitro (Gokhin et al., 2012; Nowak and Fowler, 2012; Parreno et al., 2018). A recent study has reported a comprehensive overview of age-related changes in wild-type murine lenses including lens stiffness and refractive index, suggesting similarities between murine and primate lenses (Cheng et al., 2019). Genetic mutant mice are readily available for investigating the molecular and cellular bases for the regulation of lens mechanical and optical properties.

Several studies also indicate that mouse lens stiffness is influenced by lens capsule and cellular microstructure, age and genetic backgrounds of mouse strains and gene mutations (Fudge et al., 2011; Baradia et al., 2010). Additional reports have shown that the loss of soluble α-crystallins increases the stiffness of the lens nucleus specifically (Heys et al., 2007; Truscott and Zhu, 2010; Truscott, 2009). Proteins required for proper organization of lens fiber cells have also been shown to affect lens stiffness. For instance, tropomodulin1 (Tmod1) is an actin capping protein required for the hexagonal geometry of the lens fiber cells (Yamashiro et al., 2012; Nowak et al., 2009; Fischer et al., 2000). Loss of Tmod1 in mice resulted in a decrease in load-bearing ability (Gokhin et al., 2012). Similar results were obtained upon the loss of lens-specific beaded filament CP49 (Fudge et al., 2011). These studies revealed some insights about how interactions between lens proteins, cell cytoskeleton and cell membrane could affect lens stiffness. It is necessary to study whether and how age-related lens stiffness can be impacted by the changes of gap junctions and intermediate filaments at different mouse strain backgrounds.

Various methods have been used to measure lens stiffness, such as penetrating using a conical probe (Pau and Kranz, 1991), squeezing by an actuator (Glasser and Campbell,

1998; Baradia et al., 2010), stacking several static weights on top of the lens (Gokhin et al., 2012), and spinning of lenses (Fisher, 1971; Burd et al., 2011; Wilde et al., 2012). Here, we used a highly adjustable muscle lever device to measure stiffness of lenses from mice of different age groups and genetic backgrounds. This device can provide an accurate measure of force and displacement exerted onto the lens, and stiffness values can be determined based on the measurements of displacements.

This work has investigated the changes of lens stiffness with aging by using mouse Cx46KO models with a disruption of Gja3 gene, which encodes connexin 46 (Cx46) protein subunits of gap junction channels in lens fibers. Both wild-type and Cx46KO mice at young and old ages from the C57BL/6J (B6) and 129SvJae (129) strain backgrounds were subjected to the measurement of lens stiffness by using the muscle lever device. Cell shapes of lens peripheral fibers under uncompressed and compressed states were examined by quantitative analysis of the lens morphological images. The results indicate that Cx46 plays an important role in the regulation of lens stiffness.

2. Material and methods

2.1. Mice and lens sample preparation

Mouse care and breeding were performed according to the Animal Welfare Regulations and the National Institute Health guidelines and regulations for using animal research. The Animal Care and Use Committee (ACUC) at University of California at Berkeley approved the experimental protocol with all procedures as well as animal care, monitoring and breeding for using mice in this study. Animals were housed with free access to food and water, with a 12:12 h light:dark cycle. Four mouse lines, including C57BL/6J wild-type (B6), B6-Cx46KO ($Gja3^{tm1}$), 129SvJae wild-type (129) and 129-Cx46KO ($Gja3^{tm1}$), were used in this study. Mice were euthanized by CO_2 inhalation followed by cervical dislocation. Fresh lenses were immediately dissected in phosphate buffered saline (PBS). Lens images were collected under a dissection microscope (MZ16 Leica) with a digital camera. For side images, lenses were placed near a 45° right angle mirror. All fresh lenses from mice at two different ages, young (4 weeks old) and old (40–44 weeks old), were subjected to muscle lever compression measurement.

2.2. Biomechanical compression testing using a muscle lever device

Freshly dissected mouse lenses were transferred to individual tubes and submerged in Dulbecco’s Modified Eagle Medium (DMEM) without phenol red while being transported to the muscle lever device. Each lens was placed one at a time inside a clear, plastic chamber filled with DMEM during compression testing. A hand camera was used to record lens compression during each trial and to visually confirm proper placement of the lens and the muscle lever. Mechanical testing was performed on the submerged lens surface by using a hardened clay top-piece attached to a needle connected to the muscle lever. The loading regimen used was a triangle wave with a maximum of 2 mN of force to be reached to compress the lens after 2 min. Then the lens was unloaded back to 0 mN of force in 2 min, a duration of 4 min per testing cycle. Force and displacement data were collected every 0.2 s during the testing. The lever was then raised out from the chamber, and the

lens was continually recorded up to 3 min afterwards. The Matlab vR2009b software was used to access and analyze the data generated by the muscle lever. The average and standard deviation of maximum displacement measurements were plotted in Excel.

A three-way between subjects ANOVA was used to determine the effects of mouse age, genetic background, and Cx46 genotype on muscle lever lens displacement. Once the ANOVA was determined to be significant, Scheffe post-hoc correction was used to determine which pairs of means were significant. The Scheffe correction was used due to unequal sample sizes between comparison groups. P values lower than 0.05 were considered statistically significant. The calculations were performed using the JASP statistical software package (JASP Team (2020), JASP (Version 0.14.1)).

2.3. Vibratome sections of uncompressed and compressed lenses

For each pair of lenses extracted from one mouse, one lens was fixed uncompressed, while the other lens was fixed under static compression using 16 circular glass coverslips with a diameter of 12 mm to mimic the compression experienced during the muscle lever experiments. The selection of 16 coverslips was calculated to approximately mimic the maximum compression experienced by the lens during muscle lever compression. The same set of coverslips was used for each experiment. A small piece of plastic sheet approximately 1 mm in height was positioned with super glue in the corner edge of each plastic chamber to allow the coverslips to more directly compress each lens vertically as opposed to compressing them at an angle.

Both uncompressed and compressed lenses were placed in clear, plastic chambers filled with 4% paraformaldehyde (PFA) in PBS and fixed for 1 h at room temperature. After fixation, lenses were washed in PBS three times for 10 min each. Then fixed lenses were mounted with super glue onto an aluminum-sectioning stand. Lenses were covered with warm 2.5% agar, then submerged in PBS and sectioned using a Leica VT 1000S microtome with a speed setting of 3–4 and frequency setting of 6–7. Lens cross sections between 100 and 150 μm in thickness from similar depths (near the equator of each lens) in different lens samples were collected and post-fixed for 10 min with cold 4% PFA in PBS and then washed in cold PBS three times before histochemical staining.

2.4. Morphological and statistical analysis of lens fiber cells

Lens vibratome sections were incubated with Alexa Fluor 488 Phalloidin (Thermo Fisher Scientific, Inc.) and Rhodamine wheat germ agglutinin (WGA) (Vector Laboratories, Inc., Burlingame, CA) for 2 h at room temperature in a blocking solution consisting of 3% bovine serum albumin (BSA) (Research Products International, Mt Prospect, IL), 3% normal goat serum (NGS) (Vector Laboratories, Inc., Burlingame, CA), and 0.3% Triton X-100 in PBS. Sections were then washed three times in PBS and mounted with DAPI VectorShield mounting medium (Vector Laboratories, Inc., Burlingame, CA). Florescent images were collected by a Zeiss LSM700 confocal microscope with a 63X lens. Staining was repeated at least three times from lens pairs of three different mice, and representative results were shown.

High magnification images of both uncompressed and compressed lens sections were analyzed using the ImageJ software. Rows of fiber cells were first enumerated, and each fiber cell width within a row was measured. Cells containing nuclei were omitted in the final analysis as they artificially overinflated the average fiber cell width. Two neighboring cells with one cell containing a nucleus were also omitted from the analysis as they were often pushed aside from the larger nucleus, significantly thinning their width measurement. A bounding box of 40 μm in width and 100 μm in height was drawn approximately 10 μm from the lens surface. A second bounding box with the same dimensions was stacked next to the first, creating two distinct regions of 10–50 μm from the lens surface and 50–90 μm from the lens surface. Only fiber cells fully included within each bounding box were counted. The average and standard deviation of all fiber cell width measurements within each bounding box were plotted in Excel. Student's t-test was used to determine statistical significance.

A two-way between subjects ANOVA was used to examine the effect of coverslip compression and fiber cell depth on fiber cell width. Once significance was determined using ANOVA, Scheffe post-hoc correction was used to determine which pairs of means were significant. The Scheffe correction was used due to unequal sample sizes between comparison groups. P values lower than 0.05 were considered statistically significant. The calculations were performed using the JASP statistical software package (JASP Team (2020), JASP (Version 0.14.1)).

3. Results

3.1. Young and old lenses measured by a muscle lever lens compression apparatus

As expected, lenses from wild-type mice of both B6 and 129 strain backgrounds were clear at the ages of 4 weeks (young) and over 40 weeks (old). The B6-Cx46KO lenses displayed mild cataracts while the 129-Cx46KO lenses had severe nuclear cataracts (Fig. 1), which is consistent with our previous publication (Gong et al., 1999).

The muscle lever device consists of a clay top-piece attached to a controllable lever arm of a thin metal pin. The position and/or force of the lever arm can be precisely controlled through the MATLAB software. Lens samples were submerged in warm Dulbecco's Modified Eagle Medium (DMEM) without phenol red in a clear plastic chamber with a handheld camera positioned to video record the lens during the entire compression trial, and to confirm correct positioning of the lens and the top-piece (Fig. 2A). Videos of the entire compression process and up to 3 min after the removal of the clay top were recorded for each lens sample. Representative still images at various time points throughout each trial were captured from the video files to show the lens at various stages of compression (Fig. 2B). The 3-min rest period after each compression trial was found to be enough to visually observe the lens return to its original shape. The vertical distance change of the lens surface is reported as lens displacement.

Representative displacement and force curves were presented to demonstrate the typical data obtained during muscle lever compression. The force curve (green) showed a triangle wave starting at 0 mN, peaking at 2 mN after 2 min, and then returning to 0 mN after two more minutes (Fig. 2C, top). The displacement curve (blue) reached its peak value at 2

min, coinciding with the peak in force (Fig. 2C, top). This point of maximum displacement was used to compare lenses from mice of various genotype and age groups. The data were also plotted as Force (mN) vs Displacement (μm) to help visualize additional mechanical properties of each compression trial (Fig. 2C, bottom).

3.2. Stiffness comparison between young and old lenses of different genetic backgrounds

Using the muscle lever lens compression apparatus, a decrease in average maximum displacement reflects an increase in lens stiffness. Compared to young lenses (4 weeks old) from the same genotype mice, old lenses (over 40 weeks old) in both B6 and 129 strain backgrounds appeared to be stiffer because of their significant decrease in maximum displacement. There were significant main effects for all three independent variables, age ($p < 0.001$), strain background ($p = 0.005$), and genotype ($p < 0.001$). There were also significant interactions between the effects of age and genotype ($p = 0.004$), as well as the combination of all three variables ($p < 0.001$). Young B6-WT lenses had average maximum displacement of 328.5 μm ± 18.9 μm ($n = 9$), while old B6-WT lenses displayed reduced average maximum displacement of 179.8 μm ± 17.2 μm ($n = 12$); post-hoc tests using the Scheffe correction showed that the old B6-WT lenses were significantly stiffer than young lenses ($p_{Scheffe} < 0.001$), showing about 45% reduction in lens displacement. The same trend is observed at 129 strain background, with young 129-WT lenses averaged 303.7 μm ± 20.7 μm ($n = 6$) and old 129-WT lenses averaged 242.2 μm ± 31.4 μm ($n = 12$) (Fig. 3); the old 129-WT lenses were also significantly stiffer than young lenses ($p_{Scheffe} < 0.01$), displaying about 20% reduction in lens displacement. The stiffness of young 129-WT and young B6-WT lenses were similar as their average displacements were not statistically different ($p_{Scheffe} = 0.871$). In contrast, the old 129-WT lenses were significantly softer than the old B6-WT lenses ($p_{Scheffe} < 0.001$), showing about 35% increase in lens displacement.

A deletion of Cx46 appeared to significantly stiffen lenses in young B6, old B6 and old 129 mice but not young 129 mice (Fig. 3, light bars). The maximum displacement of young B6-Cx46KO lenses averaged 251.9 μm ± 39.2 μm ($n = 16$), significantly lower than that of B6-WT lenses ($p_{Scheffe} < 0.001$), about 23% reduction; while the maximum displacement of young 129-Cx46KO lenses averaged at 287.9 μm ± 12.3 μm ($n = 8$), a value similar to that of 129-WT lenses and is not statistically different ($p_{Scheffe} = 0.990$). Differences were obvious in older lenses, with the maximum displacement of old B6-Cx46KO lenses averaged 128.6 μm ± 24.1 μm ($n = 12$), significantly lower than that of old B6-WT lenses ($p_{Scheffe} < 0.01$), about 28% reduction; the maximum displacement of old 129-Cx46KO lenses averaged 127.0 μm ± 23.2 μm ($n = 7$), significantly lower than old 129-WT lenses ($p_{Scheffe} < 0.001$) (Fig. 3A), about 50% reduction. The static significances for the comparison in Fig. 3

3.3. Changes of peripheral lens fiber cell shape during lens compression

Lenses from 4-week-old B6-WT mice were used to further investigate the cell shape changes that might be occurring during the compression of a lens. To mimic the compression of the lens during muscle lever experiments, 16 glass coverslips with a diameter of 12 mm (mimicking the maximum displacement force) were used to statically

compress the lens during fixation with 4% paraformaldehyde (Fig. 4A). After 1 h, coverslips were removed, and lenses retained compressed shapes were processed for morphological examination of lens fibers.

Two distinct regions of lens fibers with typical hexagonal shape, approximately 10–50 μm and 50–90 μm from the lens surface, were chosen to determine any potential shape changes that might be occurring during compression (Fig. 4B). Representative high magnification images from both uncompressed and compressed lenses with outlined bounding boxes were used for ImageJ analysis. The width of these lens fiber cells was chosen as the representative parameter to analyze, but other parameters, such as length, perimeter, aspect ratio, and total cross-sectional area, were also considered. The widths of individual fiber cells within each bounding box were counted and averaged for final analysis.

Statistical analysis of average fiber cell width within two chosen regions (10–50 μm and 50–90 μm) of lens sections from three different young B6 wild-type lenses (n1, n2 and n3) under uncompressed and compressed conditions was performed and summarized in Table 1. The changes of average fiber cell width of each lens sample between uncompressed and compressed conditions are obvious in the 10–50 μm region but not in the 50–90 μm region (Fig. 4C). Moreover, statistical comparisons of the average fiber cell width in the two chosen regions of three lens samples are shown (Fig. 4D). There were significant main effects for both fiber cell region ($p < 0.001$) and compression state ($p < 0.001$), as well as a statistically significant interaction effect between the two conditions ($p < 0.001$). In the 10–50 μm region, fiber cells in the uncompressed state averaged a width of 1.785 μm ± 0.403 μm, from 429 cells of three different lens samples (n = 3 lenses, 429 cells total) measured; while fiber cells in the compressed state averaged a width of 1.419 μm ± 0.301 μm (n = 3, 493 cells), shown to be significantly narrower than the uncompressed cells using Scheffe post-hoc correction ($p_{Scheffe} < 0.001$), about 20.5% reduction in width (Fig. 4D, the left pair of bars). This indicated that near the very periphery of the lens, fiber cells appeared to be stretched along their long side axis during compression. Interestingly, the opposite trend was observed in the deeper 50–90 μm region, with uncompressed fiber cells averaging a width of 2.178 μm ± 0.519 μm (n = 3, 342 cells) and compressed fibers averaging slightly wider at 2.329 μm ± 0.494 μm (n = 3, 257 cells). The average size of the compressed fibers in the deeper region was found to be significantly wider than uncompressed fibers from the same region ($p_{Scheffe} < 0.05$), despite the absolute difference being quite subtle, only a 6.9% increase. This suggested that within this deeper region, hexagonal cross-section fiber cells were being stretched along their short side axis to become square-like cross-section under compression.

The deep fibers beyond the regions above displayed waved cell boundaries and irregular shapes in the B6-WT lens sections, thus we were unable to quantitatively analyze their cell shapes. In addition, we did not observe any significant changes of peripheral fiber cell shapes between uncompressed and compressed lenses of 4-week-old B6-Cx46KO, 129-WT and 129-Cx46KO mice, besides some compressed inner fibers seemed to be wider, especially in the 129-Cx46KO lenses (Fig. 5, towards the right side on the bottom-right panel).

4. Discussion

This work provides the first in vivo evidence that the presence of Cx46 connexin is important for lens stiffness in old mice since old Cx46 KO mice show drastically increased lens stiffness regardless of mouse B6 and 129 strain genetic backgrounds. Young B6-Cx46KO lens stiffness is significantly increased when compared to B6 wild-type control, thus Cx46 is also important for lens stiffness of young mice at B6 genetic background. However, young 129-Cx46KO lens stiffness appears to be unchanged, while Old 129-Cx46KO lenses become equally hardening as old B6-Cx46KO lenses. These results indicate that Cx46 is important for the regulation of lens stiffness in old mice, regardless of the strain backgrounds.

4.1. Cx46 gap junctions and lens stiffness

Lens Cx46 and Cx50 can form homomeric and heteromeric gap junctions (Kumar and Gilula, 1996; Jiang et al., 1995). They are co-localized in the ball-and-sockets on the long side as well as in the flat regions on the short side of hexagonal shape fiber cells (Wang et al., 2016, 2017; Lo and Reese, 1993; Biswas et al., 2010). Several studies have suggested the adhesion role of Cx50 in cultured lens cells in vitro and its role in maintaining organization and integrity of lens fibers in vivo (Gu et al., 2019; Hu et al., 2017). However, the role of Cx46 gap junctions as adhesion structures between lens fibers has not been evaluated. This work suggests that the presence of Cx46 is essential for maintaining old lens stiffness. The downstream mechanism for how a loss of Cx46 leads to lens hardening remains unknown at current stage. The lens hardening occurs at similar levels in old Cx46KO lenses of both B6 and 129 strain genetic backgrounds, which contradicts the fact that age-related nuclear cataract appears to be more severe in 129 Cx46KO mice. Nuclear cataract formation in Cx46KO is associated with lens calcium elevation as well as increased degradation and aggregation of crystallin proteins; and Capn3 (calpain 3) gene deletion could alleviate nuclear cataract in 129 Cx46 CAPN3 double knockout lenses (Tang et al., 2007). Up to date, there is no study directly addressing whether lens calcium level elevation or activation of calpain3 activity are involved in the regulation of lens stiffness. Based on the outcome of lens stiffness increase in both 129 and B6 Cx46KO lenses of old mice, this study suggests that the downstream mechanism leading to lens hardening may differ, at least in part, from the mechanism that causes nuclear cataracts in Cx46KO lenses. We do not know whether the lens hardening in Cx46KO lenses is related to the function of Cx46, Cx46 hemichannels, Cx46 gap junctions and/or their downstream targets. Future studies will be needed to elucidate the molecular and cellular mechanisms that cause lens hardening in Cx46KO lenses, which may be related to interactions between gap junction communication and cytoskeletal structures.

4.2. Lens stiffness and cytoskeletons

Mechanistic studies of lens stiffness have been mainly focused on the lens cytoskeletal proteins due to their involvement in lens cell architecture and mechanical properties. The 129 wild-type mouse strain contains a CP49 gene deletion, thus abolishing lens beaded intermediate filaments (Alizadeh et al., 2004). The lens stiffness of 5- to -12-week-old CP49KO lenses are lower than their wild-type counterparts, but 1-year--old wild-type and

CP49KO lenses show similar stiffness (Fudge et al., 2011). CP49 deletion alleviates the lens stiffness increase in young 129 Cx46KO lenses but not old 129 Cx46KO lenses. This work also confirms that CP49 knockout lenses are less stiff than wild-type controls. The underlying mechanism for how an absence of CP49 leads to lens softening remains elusive. A recent study reported that Tmod1(−/−) CP49(−/−) double-knockout (DKO) disrupted cytoskeletal networks in lens fiber cells, resulting in increased gap junction coupling resistance and hydrostatic pressure (Cheng et al., 2015). Gap junction plaques, resting in voids of the membrane-associated actin-spectrin network, became smaller in size due to the disruption of actin-spectrin network in DKO fibers. It remains unclear about how impaired gap junctions in Cx46KO directly and/or indirectly affect the lens stiffness. How gap junctions and cytoskeletons coordinately regulate lens mechanical properties needs to be further investigated too.

4.3. Lens stiffness, lens fibers and aging

Several studies have linked increased lens stiffness with aging (Heys et al., 2004; Gokhin et al., 2012; Baradia et al., 2010; Burd et al., 2011). The increase of lens stiffness is greater in the human lens nucleus, which is initially softer than the surrounding cortex until about the age of 40 years when the lens nucleus becomes stiffer (Weeber et al., 2007; Michael and Bron, 2011). Our measurements were performed on whole intact lenses, which do not permit differentiation between cortex and nucleus. Fresh whole lenses were chosen in this study to avoid any destructive structural damage that would ultimately be caused by freezing or slicing of the lens. In this study, Cx46KO lenses recovered to its original size and shape after the compressed test. We were unable to obtain reliable data from dissected lens nucleus with this dynamic stiffness measurement. A new technology that can directly measure the stiffness changes of lens core will be crucial to understand the age-related increase of lens stiffness.

The morphological analysis of peripheral fibers of young B6 lenses reveals unique changes of hexagonal shape fibers under uncompressed and compressed conditions (Fig. 6). This finding is similar to a previous study that reports an increase in the long side of equatorial fiber cells in 10 μm depth of compressed lenses from 6- to 9-week-old C57BL/6J mice (Parreno et al., 2018). Those compressed fibers locate in less than 100 μm in depth from the lens surface; presumably fiber ends should be still attached to the lens capsule. However, the ends of the inside part of peripheral fibers were closer to the polar region when compared to the ends of the outside part of peripheral fibers. Perhaps, this positional difference might impact fiber cell deformation in a different way under strain.

Hexagonal shaped peripheral fibers become narrow towards the surface and become wide towards the interior under the compression in young B6 lenses (Fig. 6). Fiber cell narrowing is associated with the short sides stretching out while fiber cell widening is related to the short sides pushing inward. These phenomena suggest that the directional movements of short sides of hexagonal shaped fibers are responsible for the lens shape change under uncompressed and compressed conditions. Cx46 gap junctions are located at the flat regions between protrusions on the short sides (Lo and Harding, 1986; Wang et al., 2017). Presence of both Cx46 and CP49 seems to be important for supporting the directional movement

of the short sides of peripheral hexagonal shaped fibers of young B6-WT lenses, since such distinct changes are not observed in the 129 wild-type (lacking CP49), B6-Cx46KO and 129-Cx46KO lenses. It may be important to investigate the role of gap junctions and cytoskeletons in the mechanical induced movement of the short sides of fiber cells.

5. Conclusion

This study indicates that the Cx46 is important for lens stiffness in old mice. The mechanism of lens hardening may differ from the mechanism of nuclear cataract formation in Cx46KO lenses. Cx46 and gap junctions may play a role in lens accommodation or presbyopia. Cx46 knockout lenses may be a valuable model for mechanistic study of age-related lens stiffness.

Acknowledgements

This work was supported by National Institutes of Health Grant R01 EY013849.

References

Alizadeh A, Clark J, Seeberger T, Hess J, Blankenship T, FitzGerald PG, 2004. Characterization of a mutation in the lens-specific CP49 in the 129 strain of mouse. Invest. Ophthalmol. Vis. Sci 45 (3), 884–891. [PubMed: 14985306]

Baradia H, Nikahd N, Glasser A, 2010. Mouse lens stiffness measurements. Exp. Eye Res 91 (2), 300–307. [PubMed: 20542031]

Biswas SK, Lee JE, Brako L, Jiang JX, Lo WK, 2010. Gap junctions are selectively associated with interlocking ball-and-sockets but not protrusions in the lens. Mol. Vis 16, 2328–2341. [PubMed: 21139982]

Burd HJ, Wilde GS, Judge SJ, 2011. An improved spinning lens test to determine the stiffness of the human lens. Exp. Eye Res 92 (1), 28–39. [PubMed: 21040722]

Cheng C, Nowak RB, Gao J, Sun X, Biswas SK, Lo WK, Mathias RT, Fowler VM, 2015. Lens ion homeostasis relies on the assembly and/or stability of large connexin 46 gap junction plaques on the broad sides of differentiating fiber cells. Am. J. Physiol. Cell Physiol 308 (10), C835–C847. [PubMed: 25740157]

Cheng C, Parreno J, Nowak RB, Biswas SK, Wang K, Hoshino M, Uesugi K, Yagi N, Moncaster JA, Lo WK, Pierscionek B, Fowler VM, 2019. Age-related changes in eye lens biomechanics, morphology, refractive index and transparency. Aging (Albany NY) 11 (24), 12497–12531. [PubMed: 31844034]

Fischer RS, Lee A, Fowler VM, 2000. Tropomodulin and tropomyosin mediate lens cell actin cytoskeleton reorganization in vitro. Invest. Ophthalmol. Vis. Sci 41 (1), 166–174. [PubMed: 10634617]

Fisher RF, 1971. The elastic constants of the human lens. J Physiol 212 (1), 147–180. [PubMed: 5101807]

Fudge DS, McCuaig JV, Van Stralen S, Hess JF, Wang H, Mathias RT, FitzGerald PG, 2011. Intermediate filaments regulate tissue size and stiffness in the murine lens. Invest. Ophthalmol. Vis. Sci 52 (6), 3860–3867. [PubMed: 21345981]

Glasser A, Campbell MC, 1998. Presbyopia and the optical changes in the human crystalline lens with age. Vision Res 38 (2), 209–229. [PubMed: 9536350]

Glasser A, Campbell MC, 1999. Biometric, optical and physical changes in the isolated human crystalline lens with age in relation to presbyopia. Vision Res 39 (11), 1991–2015. [PubMed: 10343784]

Gokhin DS, Nowak RB, Kim NE, Arnett EE, Chen AC, Sah RL, Clark JI, Fowler VM, 2012. Tmod1 and CP49 synergize to control the fiber cell geometry, transparency, and mechanical stiffness of the mouse lens. PloS One 7 (11), e48734. [PubMed: 23144950]

Gong X, Agopian K, Kumar NM, Gilula NB, 1999. Genetic factors influence cataract formation in alpha 3 connexin knockout mice. Dev. Genet 24 (1–2), 27–32. [PubMed: 10079508]

Gu S, Biswas S, Rodriguez L, Li Z, Li Y, Riquelme MA, Shi W, Wang K, White TW, Reilly M, Lo WK, Jiang JX, 2019. Connexin 50 and AQP0 are essential in maintaining organization and integrity of lens fibers. Invest. Ophthalmol. Vis. Sci 60 (12), 4021–4032. [PubMed: 31560767]

Heys KR, Cram SL, Truscott RJ, 2004. Massive increase in the stiffness of the human lens nucleus with age: the basis for presbyopia? Mol. Vis 10, 956–963. [PubMed: 15616482]

Heys KR, Friedrich MG, Truscott RJ, 2007. Presbyopia and heat: changes associated with aging of the human lens suggest a functional role for the small heat shock protein, alpha-crystallin, in maintaining lens flexibility. Aging Cell 6 (6), 807–815. [PubMed: 17973972]

Hu Z, Shi W, Riquelme MA, Shi Q, Biswas S, Lo WK, White TW, Gu S, Jiang JX, 2017. Connexin 50 functions as an adhesive molecule and promotes lens cell differentiation. Sci. Rep 7 (1), 5298. [PubMed: 28706245]

Jiang JX, White TW, Goodenough DA, 1995. Changes in connexin expression and distribution during chick lens development. Dev. Biol 168 (2), 649–661. [PubMed: 7729595]

Kumar NM, Gilula NB, 1996. The gap junction communication channel. Cell 84 (3), 381–388. [PubMed: 8608591]

Lo WK, Harding CV, 1986. Structure and distribution of gap junctions in lens epithelium and fiber cells. Cell Tissue Res. 244 (2), 253–263. [PubMed: 3487382]

Lo WK, Reese TS, 1993. Multiple structural types of gap junctions in mouse lens. J. Cell Sci 106 (Pt 1), 227–235. [PubMed: 8270626]

Michael R, Bron AJ, 2011. The ageing lens and cataract: a model of normal and pathological ageing. Philos. Trans. R. Soc. Lond. B Biol. Sci 366 (1568), 1278–1292. [PubMed: 21402586]

Nandi SK, Nahomi RB, Rankenberg J, Glomb MA, Nagaraj RH, 2020. Glycation-mediated inter-protein cross-linking is promoted by chaperone-client complexes of alpha-crystallin: Implications for lens aging and presbyopia. J. Biol. Chem 295 (17), 5701–5716. [PubMed: 32184356]

Nowak RB, Fischer RS, Zoltoski RK, Kuszak JR, Fowler VM, 2009. Tropomodulin1 is required for membrane skeleton organization and hexagonal geometry of fiber cells in the mouse lens. J. Cell Biol 186 (6), 915–928. [PubMed: 19752024]

Nowak RB, Fowler VM, 2012. Tropomodulin 1 constrains fiber cell geometry during elongation and maturation in the lens cortex. J. Histochem. Cytochem 60 (6), 414–427. [PubMed: 22473940]

Parreno J, Cheng C, Nowak RB, Fowler VM, 2018. The effects of mechanical strain on mouse eye lens capsule and cellular microstructure. Mol. Biol. Cell 29 (16), 1963–1974. [PubMed: 30088796]

Pau H, Kranz J, 1991. The increasing sclerosis of the human lens with age and its relevance to accommodation and presbyopia. Graefes Arch. Clin. Exp. Ophthalmol 229 (3), 294–296. [PubMed: 1869070]

Tang Y, Liu X, Zoltoski RK, Novak LA, Herrera RA, Richard I, Kuszak JR, Kumar NM, 2007. Age-related cataracts in alpha3Cx46-knockout mice are dependent on a calpain 3 isoform. Invest. Ophthalmol. Vis. Sci 48 (6), 2685–2694. [PubMed: 17525200]

Truscott RJ, 2009. Presbyopia. Emerging from a blur towards an understanding of the molecular basis for this most common eye condition. Exp. Eye Res 88 (2), 241–247. [PubMed: 18675268]

Truscott RJ, Zhu X, 2010. Presbyopia and cataract: a question of heat and time. Prog Retin. Eye Res 29 (6), 487–499. [PubMed: 20472092]

Wang E, Geng A, Maniar AM, Mui BW, Gong X, 2016. Connexin 50 regulates surface ball-and-socket structures and fiber cell organization. Invest. Ophthalmol. Vis. Sci 57 (7), 3039–3046. [PubMed: 27281269]

Wang E, Geng A, Seo R, Maniar A, Gong X, 2017. Knock-in of Cx46 partially rescues fiber defects in lenses lacking Cx50. Mol. Vis 23, 160–170. [PubMed: 28458505]

Wang K, Pierscionek BK, 2019. Biomechanics of the human lens and accommodative system: functional relevance to physiological states. Prog. Retin. Eye Res 71, 114–131. [PubMed: 30439450]

Weeber HA, Eckert G, Pechhold W, van der Heijde RG, 2007. Stiffness gradient in the crystalline lens. Graefes Arch. Clin. Exp. Ophthalmol 245 (9), 1357–1366. [PubMed: 17285335]

Wilde GS, Burd HJ, Judge SJ, 2012. Shear modulus data for the human lens determined from a spinning lens test. Exp. Eye Res 97 (1), 36–48. [PubMed: 22326492]

Yamashiro S, Gokhin DS, Kimura S, Nowak RB, Fowler VM, 2012. Tropomodulins: pointed-end capping proteins that regulate actin filament architecture in diverse cell types. Cytoskeleton (Hoboken) 69 (6), 337–370. [PubMed: 22488942]

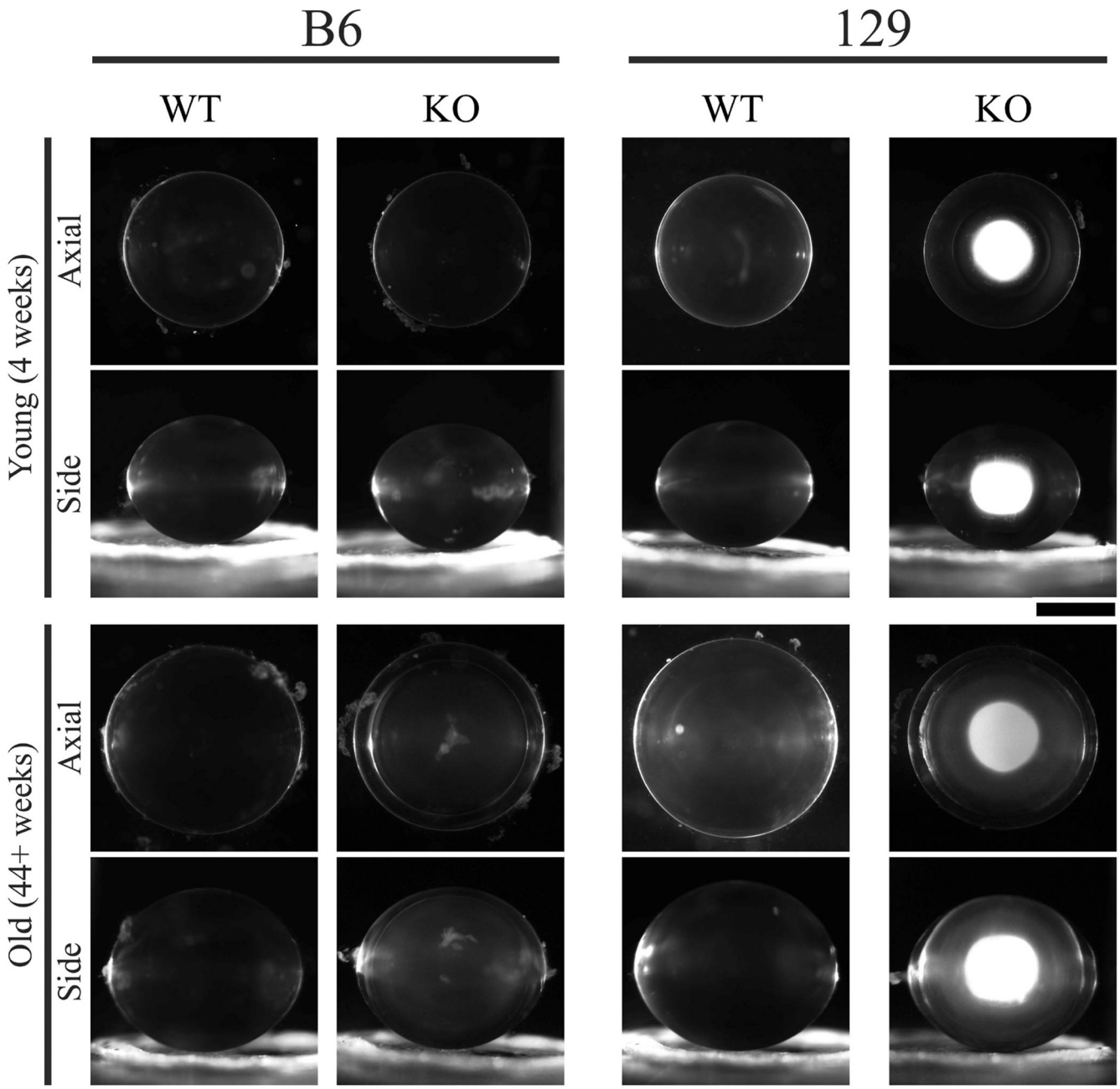

Fig. 1. Lens images of young and old WT and Cx46KO mice at B6 and 129 strain backgrounds.
Both visual axial (front) and side images of the same representative lens are shown. Young lenses (top two rows) were 4 weeks old, while old lenses (bottom two rows) were 44 weeks or older. The lenses in the left two columns were from the B6 strain background mice while the lenses in the right two columns were from the 129 strain background. Scale bar, 1 mm.

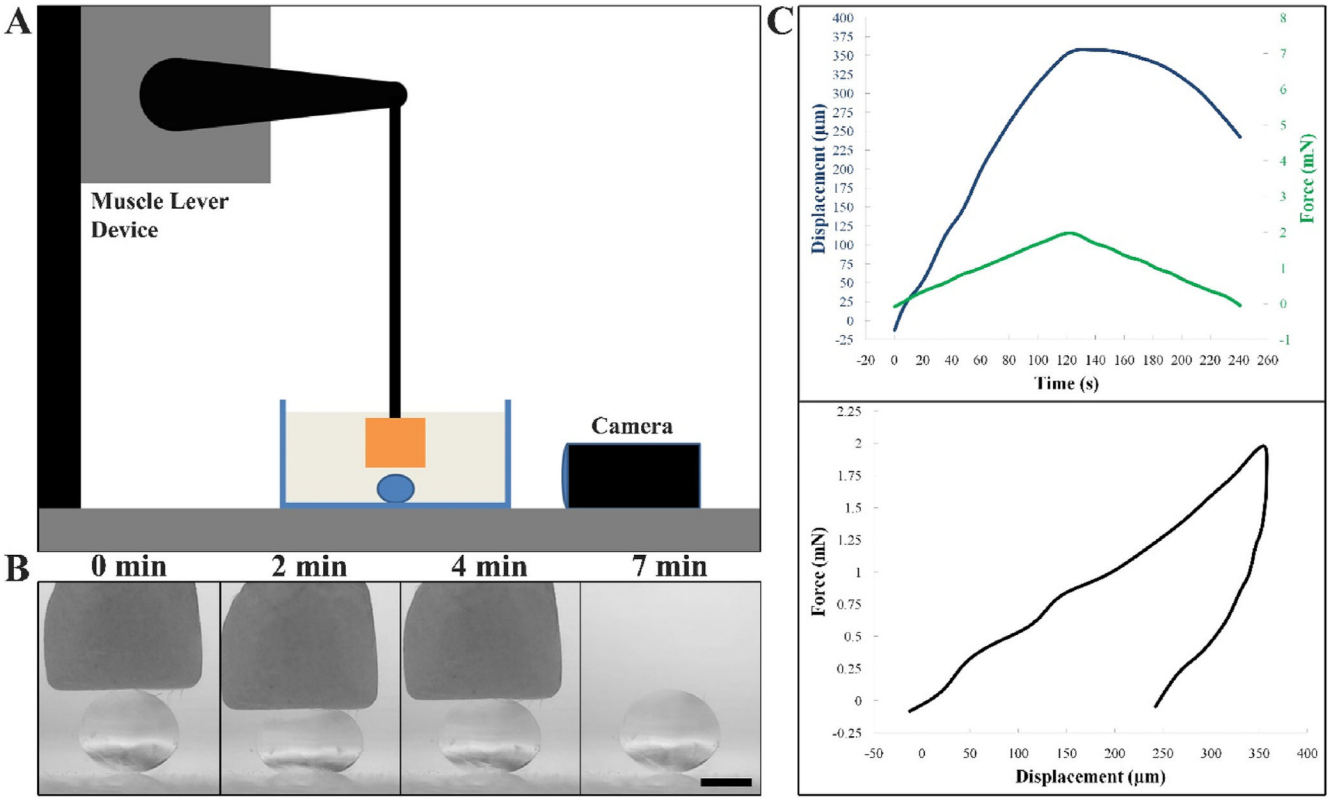

Fig. 2. Lens stiffness is measured by a muscle lever device setup.

(A) A schematic drawing shows the muscle lever system and the placement for lens sample and camera. The vertical distance change of the lens surface is reported as lens displacement. **(B)** Lens images at various time points throughout compression testing were shown: first panel, 0 min, muscle lever just barely hovering over the lens; second panel, 2 min, muscle lever was exerting the maximum force, 2 mN, and the lens was at its maximum displacement; third panel, 4 min, the muscle lever was exerting 0 mN of force and the lens was almost fully recovered to its original shape; fourth panel, 7 min, the muscle lever was removed from the lens completely, and the lens was allowed to fully recover for three additional minutes. Scale bar, 1 mm. **(C)** Representative data generated by the muscle lever system, graphed using Microsoft Excel. Top panel showed displacement (μm) (blue curve) vs time (sec) on the left axis, and force (mN) (green curve) vs time (sec) on the right axis. Bottom panel displayed force (mN) vs displacement (μm). This representative data set was taken from a 4-week-old B6-WT lens.

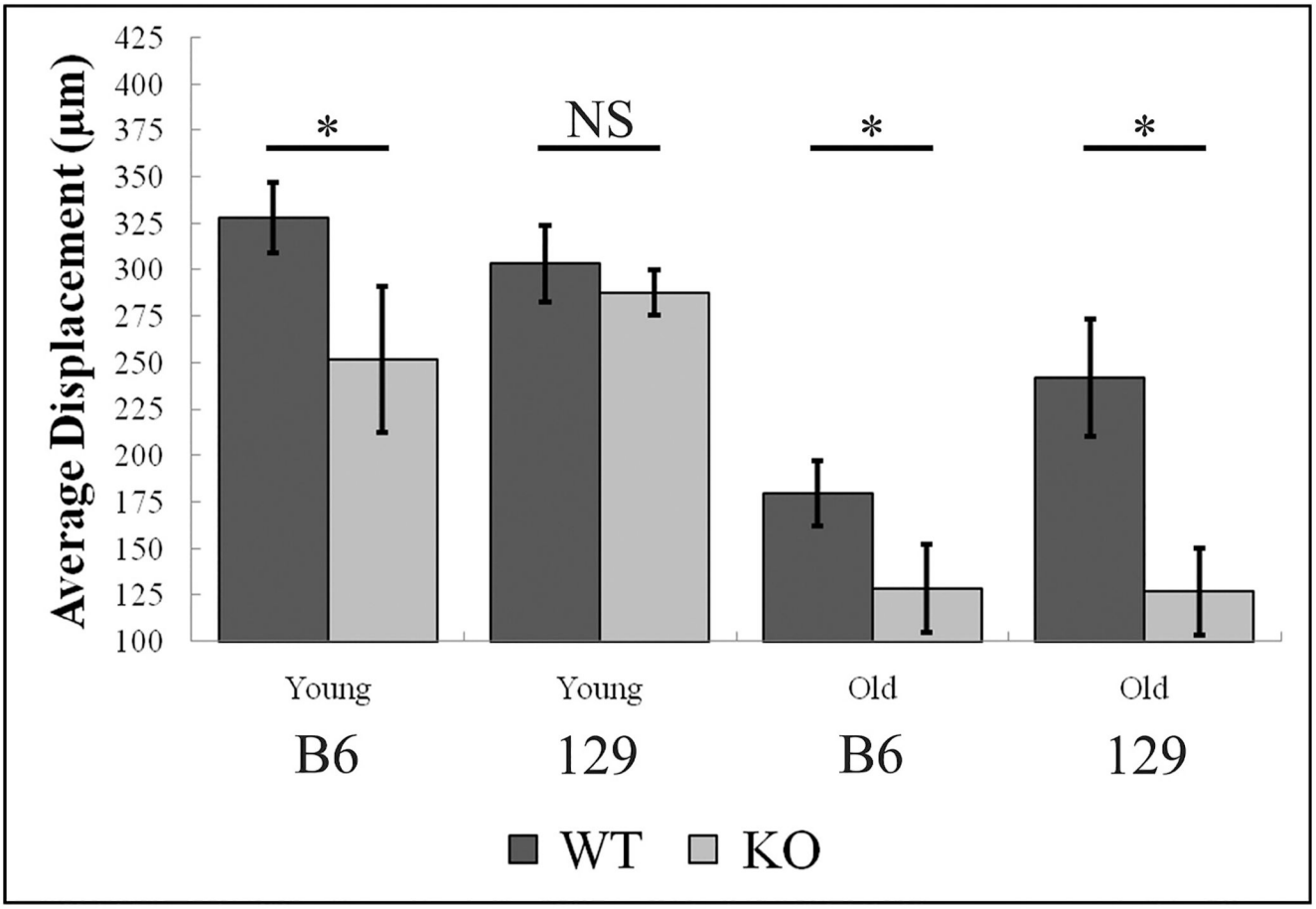

Fig. 3. Average displacement comparison between young and old lenses of WT and Cx46KO mice at B6 and 129 genetic backgrounds.

X-axis shows different lens samples, black bars for wild-type lenses and grey bars for Cx46KO samples. Y-axis shows lens average displacement with standard deviation under the maxim 2 mN of applied force. Data are mean ± SD, n = 6–12 lenses of each sample group, three-way between subjects ANOVA with post-hoc comparisons using the Scheffe test were used for statistical analysis, *$p < 0.01$, indicating a statistically significant difference between Cx46KO compared to the wild-type; NS, not statistically significant.

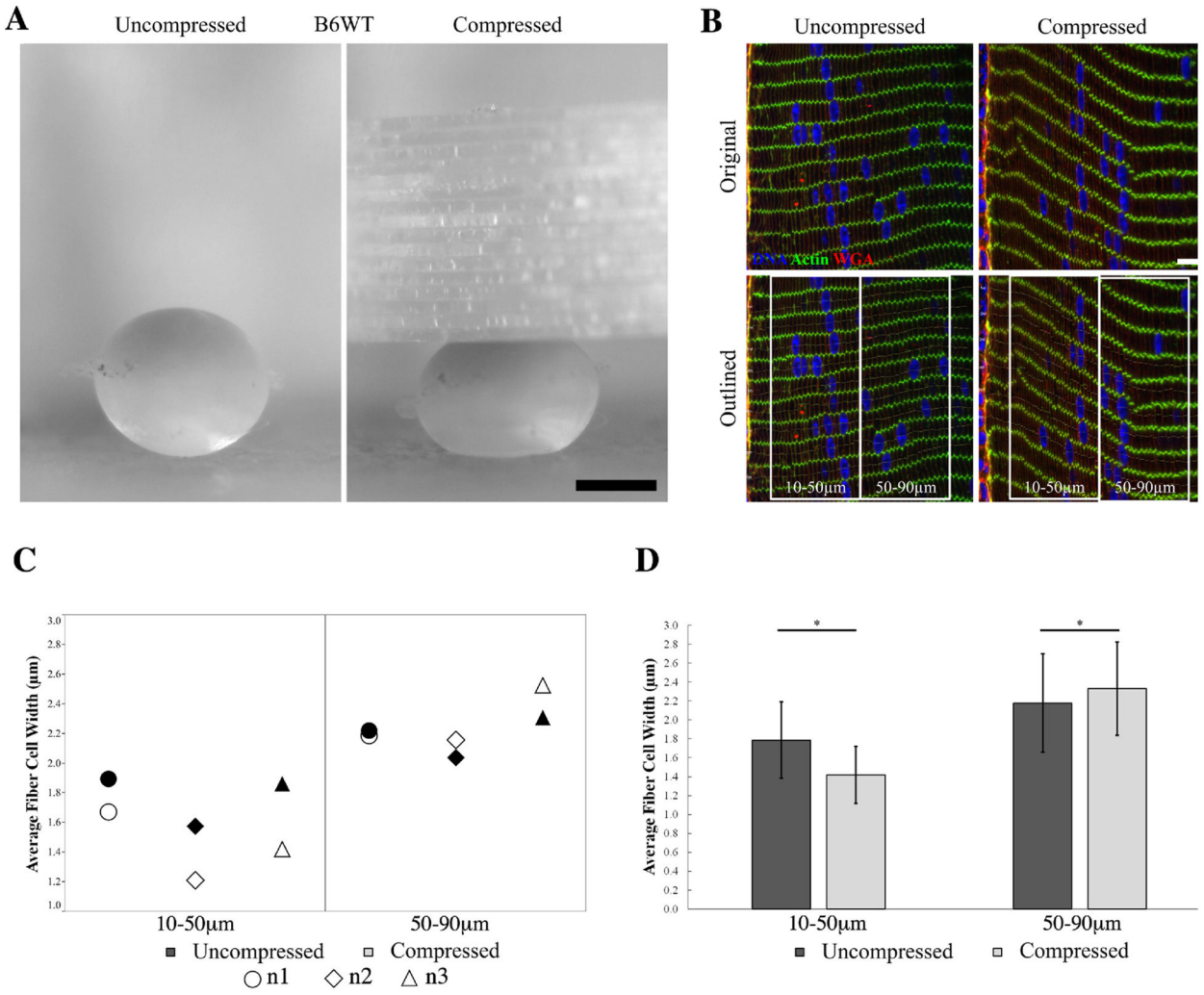

Fig. 4. Lens fiber cell shape analysis of 4-week-old uncompressed and coverslip-compressed B6-WT lenses.

(A) Side images of uncompressed lens (the left panel) before placing 16 coverslips for compressing the lens (the right panel). Scale bar, 1 mm. **(B)** Representative confocal images of lens cross vibratome sections, stained for nuclei (DAPI, blue), F-actin (FITC-phalloidin, green), and plasma membrane (rhodamine-WGA, red). The top two panels were the original uncompressed and compressed images of 100 μm-wide lens peripheral cortex (lens surface is on the left side end), and the bottom panels showed the two 40 μm-wide outlined regions in each image for measuring fiber cell widths in C. Scale bar, 10 μm. **(C)** The graphic panel shows the averages of the fiber cell width within two chosen regions (10–50 μm and 50–90 μm) of lens sections from three different young B6 wild-type lenses (n1, n2 and n3) under uncompressed and compressed conditions. **(D)** Bar graphs show the comparisons of the average fiber cell width in two regions of the lens sections between uncompressed and compressed lenses. Two-way between subjects ANOVA with post-hoc comparisons using the Scheffe test were used for statistical analysis; about 257–493 cells, from the sections of 3 different compressed and uncompressed lenses of each genotype (n = 3), were used for the comparisons, data are mean ± SD, * indicates $p < 0.05$, statistically significant.

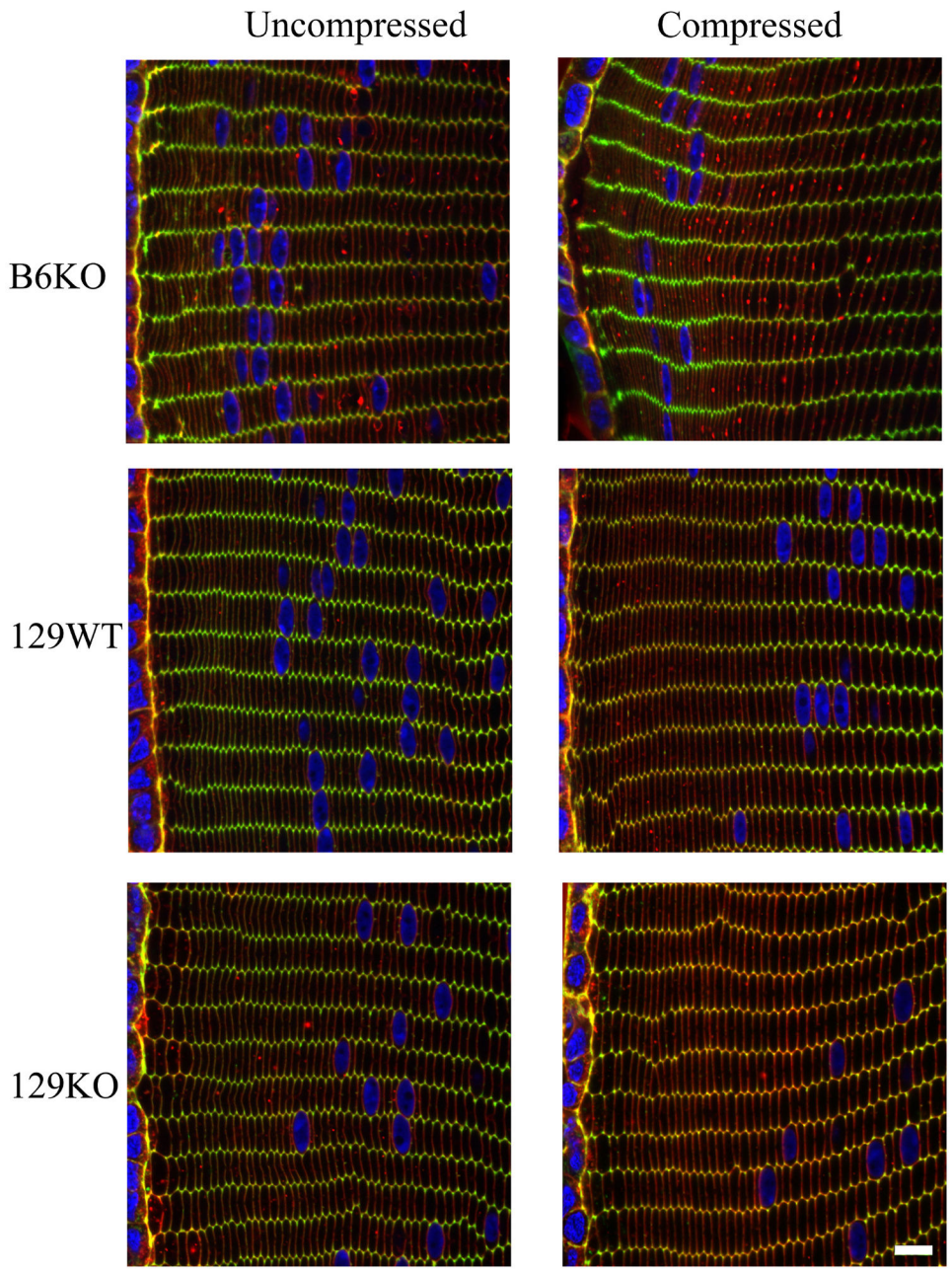

Fig. 5. Representative confocal images of lens vibratome sections of 4-week-old B6-Cx46KO, 129-WT and 129-Cx46KO lenses.

All sections were cut in the cross orientation, and stained for nuclei (DAPI, blue), F-actin (FITC-phalloidin, green), and plasma membrane (rhodamine-WGA, red). The panels displayed images of 100 μm-wide lens peripheral cortex (lens surface is on the left side end). Scale bar, 10 μm.

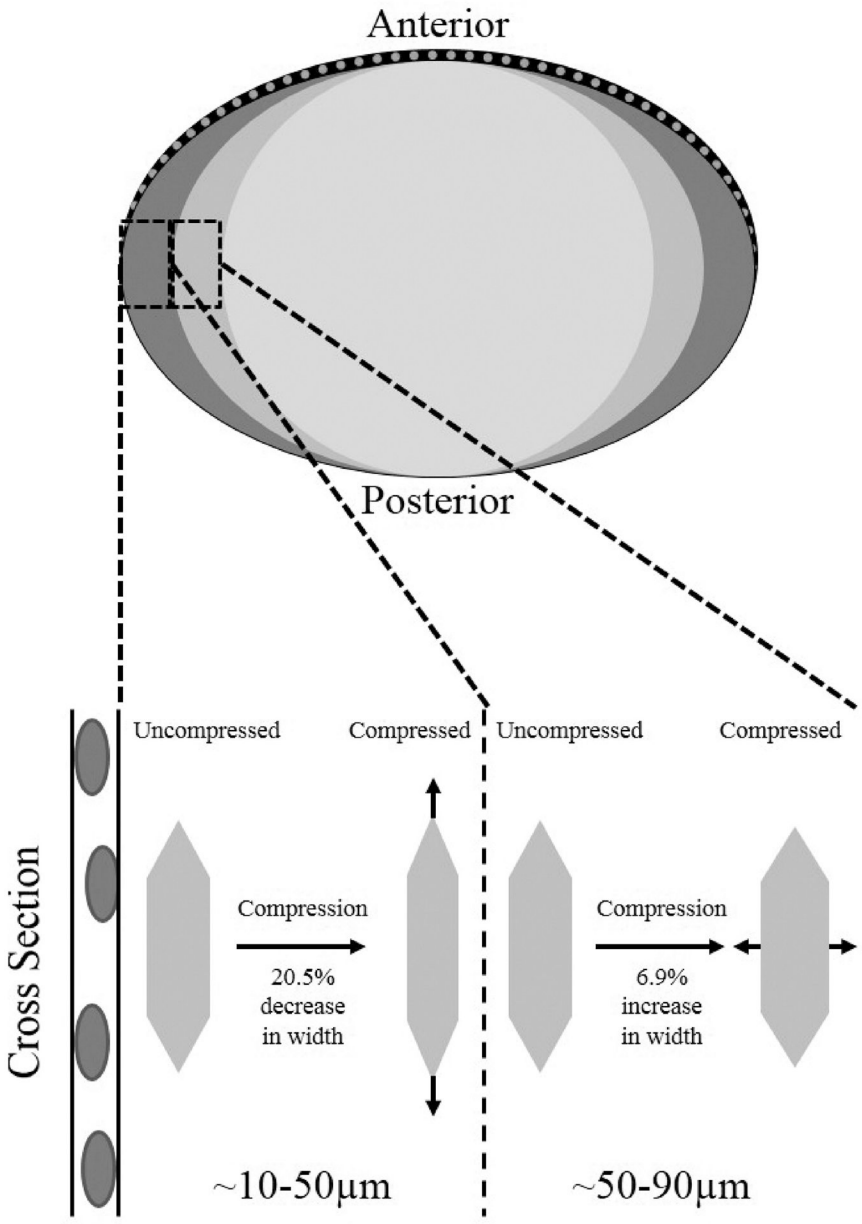

Fig. 6. A schematic summary of proposed mechanism for young B6-WT lenses.

Data presented in this study suggest that there are several bands of fiber cells when the lens was examined in an AP section: an outer band (dark grey) ranging from ~10 to 50 μm from the lens surface, an inner band (grey) in the range of ~50–90 μm, and the remainder of the fiber cell mass (light grey). Under compression, fiber cells in the light grey band region undergo a cross-sectional shape change from hexagon to square, as observed in compressed lens samples.

Table 1

Statistical analysis of average fiber cell width within two chosen regions (10–50 μm and 50–90 μm) of lens sections from three different young B6 wild-type lenses (n1, n2 and n3).

Samples	Average fiber cell width ± SD (fiber cell count)			
	10–50 μm		50–90 μm	
	Uncompressed	Compressed	Uncompressed	Compressed
n1	1.895 ± 0.378 (172 cells)	1.672 ± 0.200 (125 cells)	2.220 ± 0.682 (96 cells)	2.186 ± 0.421 (68 cells)
n2	1.576 ± 0.304 (136 cells)	1.211 ± 0.225 (155 cells)	2.038 ± 0.395 (134 cells)	2.157 ± 0.415 (74 cells)
n3	1.862 ± 0.446 (121 cells)	1.421 ± 0.284 (213 cells)	2.308 ± 0.448 (112 cells)	2.525 ± 0.514 (115 cells)
n1+n2+n3	1.785 ± 0.403 (429 cells)	1.419 ± 0.301 (493 cells)	2.178 ± 0.519 (342 cells)	2.329 ± 0.494 (257 cells)